ELSEVIER

Chemical Engineering Journal 131 (2007) 123–134

Chemical Engineering Journal

www.elsevier.com/locate/cej

Simulation of effect of catalyst particle cluster on dry methane reforming in circulating fluidized beds

Lijie Yin [a], Shuyan Wang [a], Huilin Lu [a,*], Jianmian Ding [b], Reza Mostofi [c], Zhenhua Hao [a]

[a] *School of Energy Science and Engineering, Harbin Institute of Technology, Harbin 150001, China*
[b] *Department of HYDA, IBM, Rochester, MN 55901, USA*
[c] *UOP, Des Plaines, IL 60017, USA*

Received 17 June 2006; received in revised form 2 December 2006; accepted 18 December 2006

Abstract

A study was undertaken to determine whether the performance of dry methane reforming could be affected by catalyst particle clusters in circulating fluidized bed reformers. Flow behavior and chemical reactions through a quiescent catalyst cluster were predicted. The distributions of gas temperature and concentrations of gas species were obtained using a simple two-dimensional model with Rh/Al_2O_3 catalyst particles. Numerical results show that the reforming reaction rate on catalyst particles in the cluster is much smaller than the rate on isolated catalyst particle in the stream. The molar ratio of H_2/CO is increased due to catalyst particle clustering. The effects of gas temperature, inlet gas velocity and reactor pressure on reforming reactions are also investigated.

Keywords: Dry reforming of methane; Catalyst particle cluster; Circulating fluidized bed

1. Introduction

Synthesis gas (H_2/CO) is an important feed for methanol and Fischer–Tropsch synthesis. Recently, much attention has been paid to the reaction of carbon dioxide and methane, known as dry reforming of methane because of a need for effective utilization of methane and CO_2 from natural gas [1–7]. However, CO_2 reforming is highly endothermic, and hence a highly energy intensive process [8]. A typical industrial fixed bed reformer contains an array of catalyst-filled tubes suspended in a huge furnace, supplying the heat for the highly endothermic reforming reactions. These industrial fixed bed reformers suffer from several problems which seriously affect their operation and performance [9,10]. These include low catalyst effectiveness due to internal mass transfer resistance in the large catalyst particles, low heat transfer rates, large temperature gradients and thermodynamic equilibrium constraints. A number of configurations have been tried for improving its performance, and progress has been achieved. Examples include fixed bed with hydrogen-permselective membranes [11] and catalytic oxidative steam reforming [12]. On the other hand, the fluidized bed reactor is an attractive option in the syngas production by combining combustion and reforming. This is because the fluidized bed reactor provides a high rate of heat transfer which maintains the operation isothermal and also because the permanent circulation of catalyst particles favors the burning of deposited carbon on it in the oxygen-rich zone [13–15]. As a result, the fluidized bed reactor can provide stable operation and additionally it can inhibit the formation of hot spots. However, some limitations are still associated with fluidized bed reformers, such as the fluid dynamic limitation, and the difficulty of continuous catalyst regeneration. Regardless of its limitations to improve the performance of methane reformer further, the circulating fluidized bed reformer is widely used [16–19]. The circulating fluidized bed reformer is similar, in principle, to modern fluid catalytic cracking units. The reforming catalyst is fast fluidized and reforming of methane takes place inside this catalyst bed. The deactivated catalyst is carried out of the reformer with the exit gas stream, and separated in a gas–solid separator. The carbon is completely burned and the catalyst is fully regenerated in the process and the regenerated catalyst is recycled to the riser reformer.

It is generally agreed that in a circulating fluidized bed, the suspension particles partly condense into denser clusters that

* Corresponding author.
E-mail address: huilin@hit.edu.cn (H. Lu).

1385-8947/$ – see front matter © 2007 Elsevier B.V. All rights reserved.
doi:10.1016/j.cej.2006.12.028

Nomenclature

A	cross-sectional area of cluster (m^2)
C_g	gas specific heat (kJ/(m^3 K))
C_s	coke selectivity
C_1, C_2	empirically determined constants
d	particle diameter (m)
D	molecular diffusion coefficient (m^2/s)
D_c	diameter of cluster (m)
D_{CH_4}	diffusion coefficient of CH_4 (m/s^2)
g	gravity (m/s^2)
G_k	turbulent kinetic energy production (kg/(m s^3))
G_R	production due to reaction (kg/(m s^3))
h	convective heat transfer coefficient (kJ/(m^2 s K))
ΔH_k	heat of reaction (kJ/kmol)
i, j, k	coordinate direction
k	turbulent kinetic energy (m^2/s^2)
k_A	rate constant for route (A) (mol/(kg s))
k_B	rate constant for route (B) (mol/(Pa kg s))
K	reaction rates (kmol/(m^3 s))
K_{CH_4}	adsorption equilibrium constant of CH_4 (Pa^{-1})
K_{CO_2}	adsorption equilibrium constant of CO_2 (Pa^{-1})
$\dot{m}$	mass flux rate (kg/(m^3 s))
m_P	mass of single particle (kg)
M	molar mass (kg/mol)
M_k	molecular weight of species k (g/mol)
n	particle number
p	gas pressure (Pa)
P_k	partial pressure of component k, $k = H_2$, CO, CO_2, CH_4 and H_2O (Pa)
r	radial direction (m)
R	radius of particle (m)
R_A	rate of reaction route (A) (mol/(kg s))
R_B	rate of reaction route (B) (mol/(kg s))
R_c	radius of cluster (m)
S_s	specific surface area of particle (m^2/m^3)
T_g	temperature (K)
u_g	inlet gas velocity (m/s)
u_i	mean velocity of gas phase (m/s)
u_s	particle velocity (m/s)
V	gas flux from inlet of cluster, $V_g = A \times u_g$ (m^3/s)
V_g	gas flux through cluster, $V_g = A \times u$ (m^3/s)
x	vertical coordinate (m)
Y_k	mass fraction of species k

Greek symbols

ε_g	porosity
ε	energy dissipation rate (m^2/s^3)
λ_g	thermal conductivity of gas (kJ/(m s K))
μ_g	gas viscosity (kg/(m s))
μ_l	laminar gas viscosity (kg/(m s))
ρ_g	gas density (kg/m^3)
ρ_s	particle density (kg/m^3)
σ	empirically determined constant

Subscripts

A, B	reaction routes
g	gas phase
R	at particle surface
s	solid phase

move upwards through the center of riser. At some point, they get swept towards the low velocity region near the wall, where clusters reverse their flow direction and falling along the wall [20]. Many experiments have been performed to obtain the flow behavior of clusters in circulating fluidized beds. Chen [21] obtained the cluster formation time, time fraction of existence, occurrence frequency and cluster distribution using capacitance-probe measurements of instantaneous local solid concentration in a riser. Horio and Kuroki [22] obtained the cluster velocity and time fraction in the circulating fluidized bed. Moortel et al. [23] carried out flow visualization studies of heterogeneous structures of particles and measured cluster velocities in circulating fluidized beds. Noymer and Glicksman [24] measured the velocity and wall contact times of clusters using thermal image velocimetry. Sharma et al. [25] investigated the effect of particle size and superficial velocity on the flow behavior of clusters. Manyele et al. [26] determined the cluster frequency, average solids concentration in cluster, and cluster dimension from a capacitance probe measuring transient fluctuations of local solid concentrations. The formation of particle clusters has been suggested as one of the key contributing factors on the performance of circulating fluidized bed reactors. Hence, knowledge of the properties of catalyst particle clusters is useful in predicting flow behavior and reactor performance in the circulating fluidized bed reformers.

In this work, we point our attention mainly to the influence of catalyst particle clustering on methane conversion from a theoretical point of view. CO_2 reforming of methane with a Rh/Al_2O_3 catalyst particle cluster or an isolated Rh/Al_2O_3 catalyst particle in the stream was analyzed by a simple two-dimensional model. The numerical model is capable of predicting air flux passing through a catalyst cluster, distributions of gas temperature and concentrations of gas species in the Rh/Al_2O_3 catalyst particle cluster. The effects of gas temperature, inlet gas velocity and reactor pressure on methane reforming performance have been analyzed.

2. Mathematical modeling and reaction kinetics

Fig. 1 shows the geometry of the cluster in the quiescent condition. A cluster is modeled as a round two-dimensional disk distributed in the riser. The radius of the cluster disk is R_c. Gas flow is passing through the cluster. We assumed that: (1) particles in the cluster are uniformly distributed in space, and remain quiescent. (2) The particles are assumed to be spherical, and particle diameter remains constant during reforming. (3) Radiation heat transfer between gas and particle are neglected due to small temperature difference and for simplicity, and radiation heat transfer

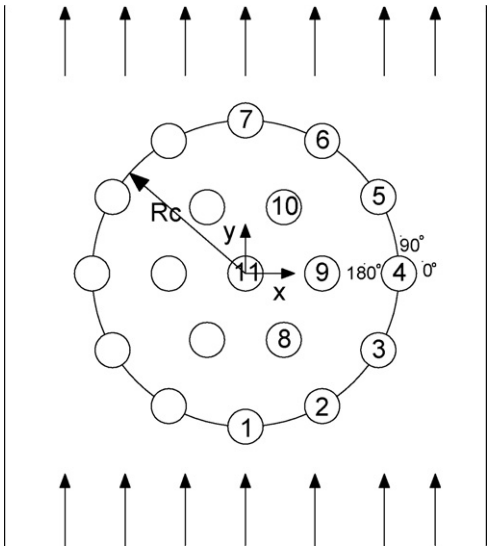

Fig. 1. Configuration of computational regime.

between particle and the walls are not accounted in the present study. Considering these assumptions, the conservation equations of mass, species and energy in Eulerian coordinates are given as follows.

2.1. Gas phase continuity equation

The mass conservation equation of gas can be written as follows [27–30]:

$$\frac{\partial}{\partial t}\rho_{\mathrm{g}} + \frac{\partial}{\partial x_j}(\rho_{\mathrm{g}} u_j) = -\sum_k \dot{m}_k \tag{1}$$

The term at right-hand side of Eq. (1) expresses mass source from CO_2 reforming reaction of methane.

2.2. Gas phase momentum equation

The conservation of momentum for gas phase is expressed as follows:

$$\frac{\partial}{\partial t}(\rho_{\mathrm{g}} u_i) + \frac{\partial}{\partial x_j}(\rho_{\mathrm{g}} u_j u_i) = \frac{\partial p}{\partial x_i} + \frac{\partial}{\partial x_j}\left(\mu_{\mathrm{g}} \frac{\partial u_j}{\partial x_i}\right) + \frac{\partial}{\partial x_j}\left(\mu_{\mathrm{g}} \frac{\partial u_i}{\partial x_j}\right) + \rho_{\mathrm{g}} g - u_i \sum_k \dot{m}_k \tag{2}$$

where $\mu_{\mathrm{g}} = \mu_{\mathrm{l}} + \mu_{\mathrm{t}}$ is the effective viscosity, $\mu_{\mathrm{t}} = C_\mu \rho_{\mathrm{g}} k^2/\varepsilon$ the gas phase turbulent viscosity and k and ε are the turbulent kinetic energy and dissipation rate. The values of the kinetic energy and dissipation rate are computed from k–ε turbulence model. The last term at right-hand side of Eq. (2) accounts for source from catalytic reactions.

2.3. Turbulence model for gas phase

There have been several approaches to model the turbulence shear stress for single phase flow [31]. From Boussinesq approximation, the shear stress is related to the turbulence parameters of the flow [32]. In present study, we employ the standard k–ε turbulence model for simulating turbulent flow. The standard k–ε turbulence model gives turbulent kinetic energy for the gas phase

$$\frac{\partial}{\partial t}(\rho_{\mathrm{g}} k) + \frac{\partial}{\partial x_j}(\rho_{\mathrm{g}} u_j k) = \frac{\partial}{\partial x_j}\left(\frac{\mu_{\mathrm{g}}}{\sigma_k}\frac{\partial k}{\partial x_j}\right) + G_k - \rho_{\mathrm{g}}\varepsilon + G_{\mathrm{R}} \tag{3}$$

and turbulent kinetic energy dissipation rate

$$\frac{\partial}{\partial t}(\rho_{\mathrm{g}} \varepsilon) + \frac{\partial}{\partial x_j}(\rho_{\mathrm{g}} u_j \varepsilon) = \frac{\partial}{\partial x_j}\left(\frac{\mu_\varepsilon}{\sigma_\varepsilon}\frac{\partial \varepsilon}{\partial x_j}\right) + \frac{\varepsilon}{k}[C_1 G_k - C_2 \rho_{\mathrm{g}}\varepsilon] + \frac{\varepsilon}{k} C_1 G_{\mathrm{R}} \tag{4}$$

where G_k is the production term,

$$G_k = \mu_{\mathrm{g}}\left(\frac{\partial u_i}{\partial x_j} + \frac{\partial u_j}{\partial x_i}\right)\frac{\partial u_i}{\partial x_j} - \frac{2}{3}\delta_{ij}\frac{\partial u_k}{\partial x_k} \tag{5}$$

and $G_{\mathrm{R}} = -k\sum_k \dot{m}_k$ is the production term from reforming. The empirical constants, σ_ε, C_μ, C_1 and C_2, are listed in Table 1.

Table 1
Parameters used in the simulations

Inlet gas velocity (m/s)	1.0
Total pressure (MPa)	0.1
Inlet gas temperature (K)	723
Inlet ratio of molar fraction	CH_4:CO_2:N_2 = 1:1:2, CH_4:CO_2:N_2 = 3:2:5, CH_4:CO_2:N_2 = 3:1:4
Inlet mass fraction of CH_4	0.139, 0.174, 0.2157
Inlet mass fraction of CO_2	0.378, 0.319, 0.2353
Inlet mass fraction of N_2	0.483, 0.507, 0.549
Gas density (kg/m^3)	0.478
Diffusion coefficient of H_2O (m^2/s)	2.178×10^{-5}
Diffusion coefficient of CO_2 (m^2/s)	1.381×10^{-5}
Empirically determined constant C_1	1.44
Empirically determined constant C_μ	0.09
Empirically determined constant σ_ε	1.3
Diameter of particle (μm)	100
Size of cluster (μm)	975
Number of particles	19
Mass of particle (kg)	2.042×10^{-9}
Temperature of particle (K)	723
Particle density (kg/m^3)	3900
Porosity of cluster	0.8
Gas viscosity (kg/m s)	3.406×10^{-5}
Diffusion coefficient of H_2 (m^2/s)	6.34×10^{-5}
Diffusion coefficient of CH_4 (m^2/s)	2.064×10^{-5}
Empirically determined constant C_2	1.92
Empirically determined constant σ_k	1.0
Empirically determined constant σ_{h}	1.0

2.4. Energy conservation of gas phase

The energy balance equation of gas phase is written as follows [30,31]:

$$\frac{\partial}{\partial t}(C_g T_g) + \frac{\partial}{\partial x_j}(u_j C_g T_g) = \frac{\partial}{\partial x_j}\left[\left(\frac{\lambda_g}{C_g} + \frac{\mu_g}{\rho_g \sigma_h}\right)\frac{\partial}{\partial x_j}(C_g T_g)\right] + h(T_p - T_g) + \sum_k \rho_s R_k \Delta H_k \quad (6)$$

where h is the gas-particle convective heat transfer coefficient [29] and R_k is the chemical reaction rate of species k. As stated before, radiation heat transfer process is not accounted in Eq. (6).

2.5. Species conservation equation

The mass balance for a gas species k (k = CO, CO_2, H_2, H_2O and CH_4) is [30–32]:

$$\frac{\partial}{\partial t}(\rho_g Y_k) + \frac{\partial}{\partial x_j}(\rho_g u_j Y_k) = \frac{\partial}{\partial x_j}\left(\rho_g D_k + \frac{\mu_g}{\sigma_Y}\right)\frac{\partial Y_k}{\partial x_j} + \sum_k \rho_s M_k R_k \quad (7)$$

where Y_k is the local mass fraction of species k, D_k the molecular diffusion coefficient and σ is the turbulent Schmidt number ($\sigma = 0.7$). The last term at right-hand side of Eq. (7) is production/dissipation rate of species k due to reaction.

2.6. Reaction kinetics

A mathematical model was used to simulate the catalytic reforming reaction with methane in a circulating fluidized bed riser. This study utilized the kinetics obtained by Richardson and Paripatyadar [33] for dry reforming on a Rh/Al_2O_3 catalyst. The reaction is the dry reforming reaction of methane with carbon dioxide [34]:

$$CH_4 + CO_2 = 2CO + 2H_2, \quad \Delta H_{298} = 247\,\text{kJ/mol} \quad (A)$$

and the reverse water–gas shift reaction:

$$CO_2 + H_2 = CO + H_2O, \quad \Delta H_{298} = 41.1\,\text{kJ/mol} \quad (B)$$

The reaction rate expressions developed by Jianquo and Froment [35] was used to estimate the individual reaction rates. The functional forms of these expressions are [16,19,36]

$$R_A = k_A \left[\frac{K_{CO_2} K_{CH_4} P_{CO_2} P_{CH_4}}{(1 + K_{CO_2} P_{CO_2} + K_{CH_4} P_{CH_4})^2}\right] \times \left[1 - \frac{(P_{CO} P_{H_2})^2}{k_A P_{CH_4} P_{CO_2}}\right] \quad (8)$$

$$R_B = k_B P_{CO_2}\left[1 - \frac{P_{CO} P_{H_2O}}{k_B P_{CO_2} P_{H_2}}\right] \quad (9)$$

The rate constant of reaction routes (A) and (B) are [16]

$$k_A = 1290 \exp\left[\frac{-102065}{R_g T_g}\right] \quad (10)$$

$$k_B = 1.856 \times 10^{-5} \exp\left[\frac{-73105}{R_g T_g}\right] \quad (11)$$

and absorption equilibrium constants of CO_2 and CH_4 are

$$K_{CO_2} = 2.64 \times 10^3 \exp\left[\frac{37641}{R_g T_g}\right] \quad (12)$$

$$K_{CH_4} = 2.63 \times 10^3 \exp\left[\frac{40684}{R_g T_g}\right] \quad (13)$$

Soliman et al. [37] have used this kinetic model for simulation of many industrial methane reforming plants and obtained a quite good agreement between the model results and plant operating data. Dissanayake et al. [38] have examined the oxidation state and phase composition of the Ni/Al_2O_3 catalyst as a function of axial position in the catalyst bed. Jin et al. [39] have provided a set of kinetic rate equations for the oxidative reforming of methane over a Ni/Al_2O_3 catalyst.

2.7. Boundary conditions and simulation procedures

The gas compositions, temperature and velocity were specified at the inlet. At the outlet, the continuous gas flow boundary condition was used. No-slip boundary conditions for gas flow at the particle surface and walls are applied:

$$u = k = \varepsilon = 0 \quad (14)$$

The surface reaction modeling is to compute concentrations of gas species at the wall. Assuming that, on a reacting surface, the mass flux of each gas species is balanced with its rate of production/consumption, then the wall surface reaction boundary conditions of gas species can be expressed as follows:

$$-D_k \left.\frac{\partial Y_k}{\partial x_j}\right|_R = \frac{\sum_k M_k R_k}{S_s} \quad (15)$$

The boundary condition of temperature at the particle surfaces is:

$$-\lambda_g \left.\frac{\partial T_g}{\partial x_j}\right|_R = \frac{\rho_s}{S_s}\sum_k R_k \Delta H_k \quad (16)$$

The governing Eqs. (1)–(7) coupling with reaction kinetics were solved with appropriate boundary conditions. The porous structure of a particle cluster was assumed to have specified porosity, $\varepsilon_g = (D_c^2 - n d_p^2)/D_c^2$, in the simulations as shown in Fig. 1. The parameters used in the simulations are listed in Table 1. The physical domain of cylindrical boundary of each particle is mapped onto a square of the computation domain using the body-fitted coordinate to make the grids fit the boundary of particles [40]. Nineteen Rh/Al_2O_3 catalyst particles form the cluster and give a cluster porosity of 0.8. These Rh/Al_2O_3 catalyst particles are assumed to be stationary. Fresh mixture of CH_4 and CO_2 gases and inert gas N_2 flow into the cluster,

react in the presence of Rh/Al_2O_3 catalyst particles, and produce gaseous species H_2, CO and H_2O and move out of the cluster. Each simulation needs about 24 h of CPU time to reach the convergence on a PC (80 GB hard disk, 128 MB Ram and of 600 MHz CPU).

3. Simulation and analysis

3.1. Base case simulations

In the base simulations, the inlet gas velocity, inlet gas temperature, porosity and reactor pressure were set to be 1.0 m/s, 723 K, 0.8 and 0.1 MPa, respectively, except specified otherwise.

Fig. 2 shows the axial velocity of gas phase at various positions. A small amount of gas flows through the cluster, while most of the gas bypasses it because of high fraction of Rh/Al_2O_3 catalyst particles in the cluster. The axial velocity of gas phase is negative behind the cluster, which means there exists a gas back flow. In reality the cluster may deform and change its shape which should have an intensive effect on gas flow in the wake region.

Ratios of air flux through the cluster to inlet air flux as a function of porosity are shown in Fig. 3 at the inlet velocity of 1.0 m/s corresponding to cluster diameter based Reynolds numbers of 64.1 and 13.6 at the inlet gas temperature of 293 and 723 K. Simulations were also performed using laminar model of gas flow. The air flux calculated from laminar model is slightly higher than from k–ε turbulent model. Under such condition, the laminar model is not worse due to less computer times used in comparison with turbulent model. Moran and Glicksman [41] modeled this system using Adina-F CFD program at the inlet gas temperature of 293 K. Both present simulations and Moran and Glicksman's results show that as the porosity approaches zero the air flux passing through the cluster goes to zero since the cluster becomes a solid disk. With the increase of porosity, the ratio of air flux is increased. As the porosity goes to one, the ratio of air flux will approach to unity. From Fig. 3 we see that at the porosity of about 90–95% the ratio of air flux passing through the cluster is exponentially increased. At a relatively high porosity level of 90% the velocity through the cluster is only 0.14 and 0.046 m/s at the inlet gas temperatures of 293 and 723 K which are an order of magnitude less than the oncoming free stream velocity. As the inlet gas temperature increases, the velocity through the cluster decreases due to high shear viscous force caused by gas viscosity.

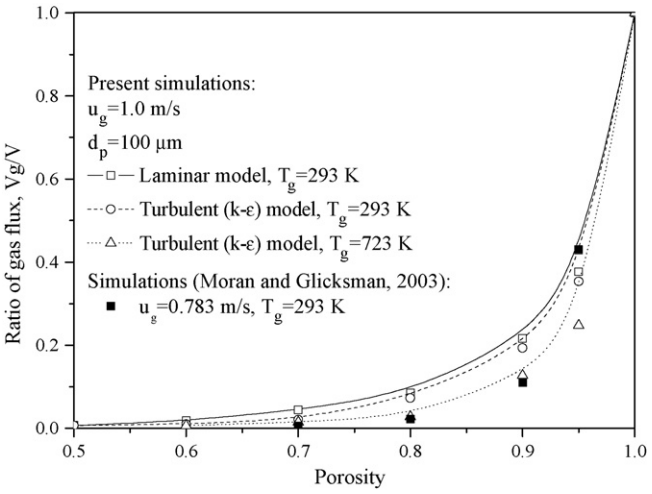

Fig. 3. Ratio of gas flux through cluster to the total air flux as a function of porosity in the cluster.

The total force acting on the particle surface is the summation of pressure force component and viscous force component. Fig. 4 shows the variation of total force acting on each particle in the cluster. The force acting on an isolated particle is also shown in this figure. The total force is different for each particle in the cluster. The force acting on particle in the cluster is always smaller than that of isolated particle in stream. At the high inlet gas temperature the force acting on each particle in cluster is always smaller than that at low inlet gas temperature due to low gas velocity inside cluster. As expected, the highest forces on particles are those face the stream and the lowest are those located at the backside of cluster. Each particle in the cluster is subject to different force acting on it varying about 10 times in magnitude.

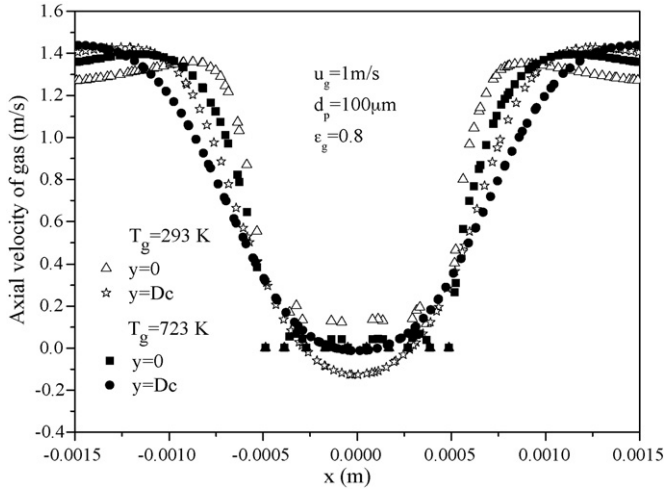

Fig. 2. Profile of gas velocity in the cluster.

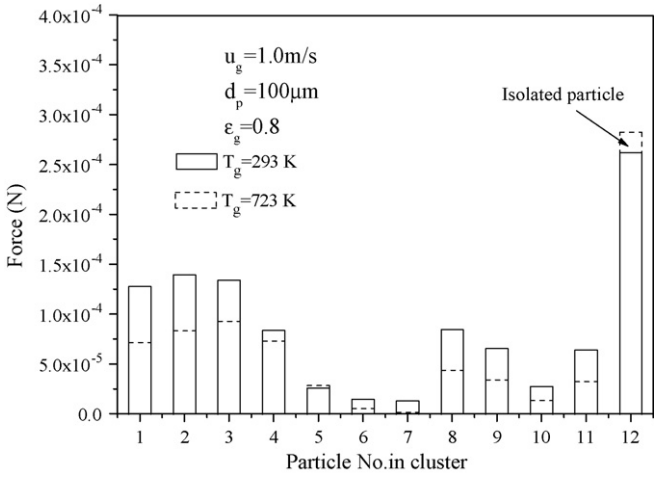

Fig. 4. Profile of force acting on the particle in the cluster and an isolated particle.

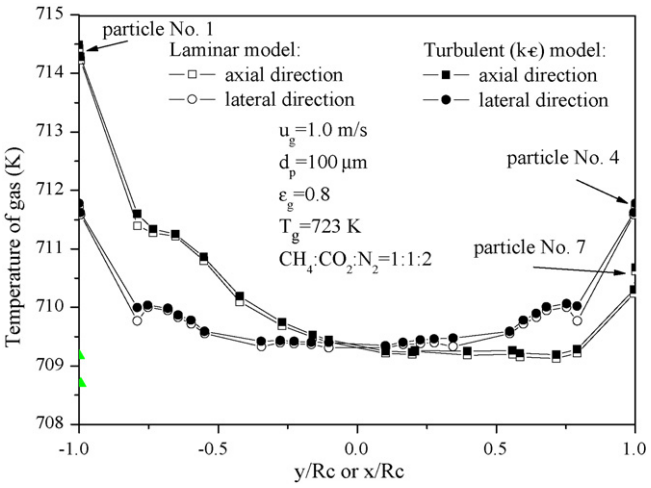

Fig. 5. Profile of gas temperature along axial and lateral directions.

Fig. 5 shows the temperature distribution of Rh/Al_2O_3 catalyst particles cluster. The gas temperature decreases through the cluster due to endothermic reaction of dry methane reforming. The high gas temperature is located at the foreside of cluster, and the low gas temperature is at the backside of cluster. In the radial direction, the gas temperature increases radially because of high temperature of fresh flowing gas. The particles facing the gas stream (those outside of the cluster) are heated by the incoming gas flow which has higher temperature than the particles. The particles, at the backside of the cluster have less convective heat transfer than those at the front side of the cluster and therefore have lower temperature than others. At the back of cluster, the gas temperature increases because of gas back mixing at the wake of particle cluster.

Fig. 6 shows the axial and radial distributions of H_2, CO and H_2O gas species along the centerline of Rh/Al_2O_3 catalyst particles cluster. The H_2 concentration decreases, while H_2O increases along flow direction due to the reverse water–gas shift reaction (B). CO concentration is very high at the tail of cluster due to the reactions (A) and (B). From this figure we see that the methane reforming reactions varies spatially within the cluster.

Fig. 7 shows the concentration distributions of H_2, CO and H_2O species for each particle in the Rh/Al_2O_3 catalyst particles cluster. The produced CO gas species is increased for each catalyst particles in cluster due to reactions (A) and (B). While the increase of H_2O concentration is due to reaction (B). For H_2 concentration, the distributions are very complex for each particle in cluster due to both the reforming reaction of methane with carbon dioxide and reverse water–gas shift reaction. Comparing with the isolated particle, the H_2, CO and H_2O concentrations of each particle in the cluster are higher. This indicates that the reforming reactions using catalyst particles are affected by the formation of particle agglomeration in the circulating fluidized bed reformer.

3.2. Effect of porosity of cluster

Fig. 8 shows the produced mass flux of H_2, CO and H_2O species as a function of porosity with two different feeding mixtures. By increasing the porosity, more gas is passing through the cluster and results in the reaction rate increase. Hence, the mass flux of H_2, CO and H_2O species are increased with the increase of porosity. This indicates that the productions of H_2, CO and H_2O species are reduced due to particle clustering. Gadalla and Sommer [42] pointed out that the production of alkanes from synthesis gas in the presence of the water–gas shift reaction requires H_2/CO ratios of less than unity. Tsipouriari and Verykios [43] showed that the water–gas shift reaction is extremely rapid under typical methane reforming conditions.

Fig. 9 shows the molar ratio of H_2/CO as a function of porosity. The computed conversion of CH_4, $(W_{CH_4,inlet} - W_{CH_4,out})/W_{CH_4,inlet}$, is also shown in this figure, where, $W_{CH_4,inlet}$ and $W_{CH_4,out}$ are the inlet and out molar fractions of methane. The molar ratio of H_2/CO and the conversion of methane decreased with the increase of porosity. Dry reforming of methane can contribute to the production of CO-rich syngas because the composition of syngas in reaction (A) is $H_2/CO = 1$. However, the production of synthesis gas from methane and carbon dioxide is influenced by the simultaneous occurrence of the reverse water–gas shift reaction (B) resulting in H_2/CO ratios less than unity. This indicates that the performance of carbon dioxide reforming with methane is varied by the formation of catalyst particle agglomeration.

3.3. Effect of gas temperature

Increasing the operating temperature has a positive effect on both the reforming reaction of methane with carbon dioxide and reverse water–gas shift reaction, since both reaction rates depend on temperature. The profile of yield of H_2, CO and produced

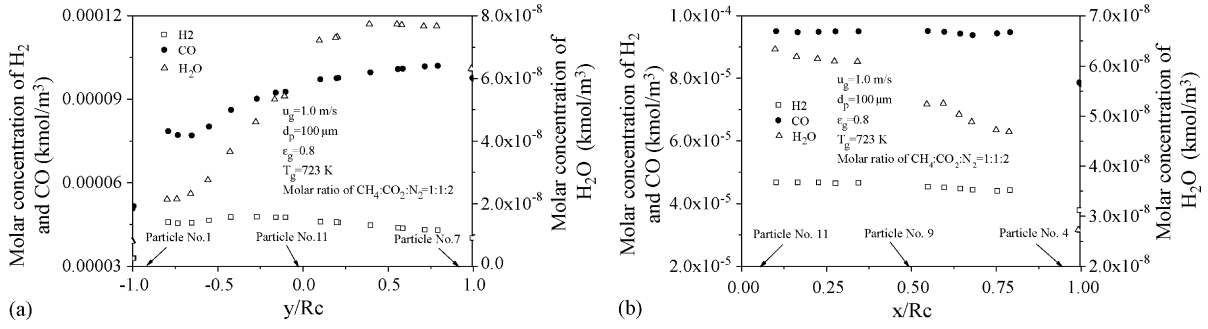

Fig. 6. Profile of molar concentration of H_2, CO and H_2O along axial and lateral directions.

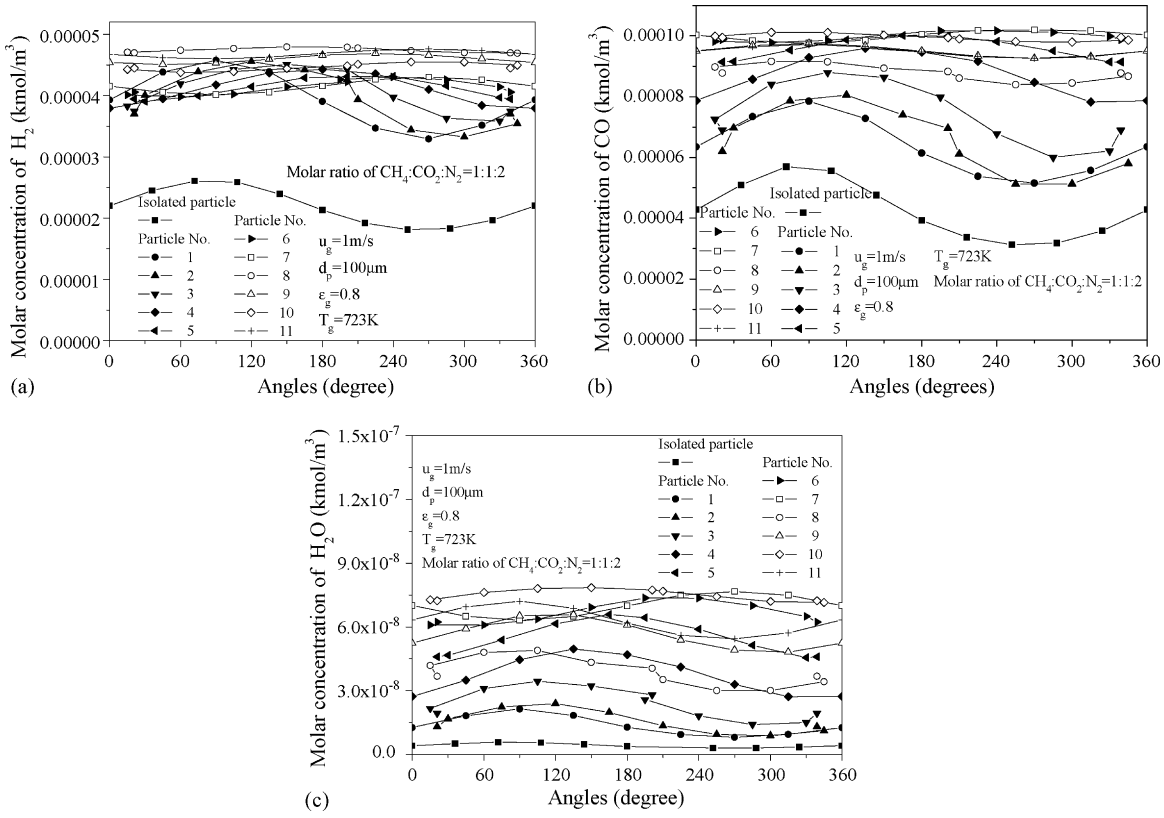

Fig. 7. Profile of molar concentration of H_2, CO and H_2O as a function of angles.

H_2O is shown in Fig. 10 as a function of inlet gas temperature. The increase in adsorption equilibrium constant with increasing gas temperature results in the increase in reaction rate constant. Therefore, the yields of hydrogen and carbon monoxide increase with increasing inlet gas temperature as expected, while the H_2O production is also increased with the increase of inlet gas temperature. Methane conversion was somewhat less than expected from equilibrium considerations due to reverse reaction.

Fig. 11 shows the molar ratio of H_2/CO as a function of inlet gas temperature. The molar ratio of H_2/CO first increases, reaches a maximum, and then decreases with increasing inlet gas temperature. At low inlet gas temperature, the reaction route (A) is faster than route (B). The production of mass flux of H_2 rises faster than that of CO. However, the reverse water–gas shift reaction is promoted at the high inlet gas temperature. These results indicate that the reaction is kinetically controlled in the investigated range of reaction conditions. Since the carbon dioxide reforming with methane and the reverse water–gas shift reaction are highly endothermic, this is a highly energy intensive process. That is, the circulating fluidized bed reformer should be heated externally to raise the temperature of the reaction mixture to achieve better selectivity.

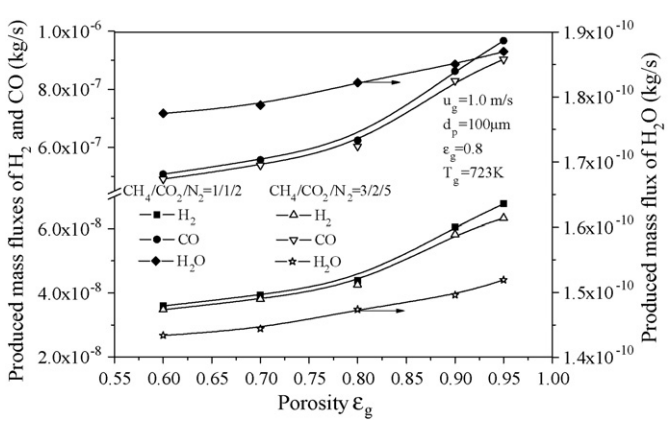

Fig. 8. Profile of produced mass flux of H_2, CO and H_2O as a function of porosity of cluster.

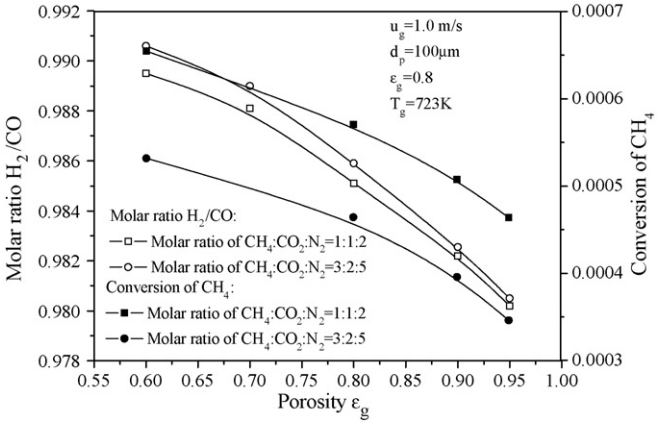

Fig. 9. Distributions of molar ratio of H_2/CO and conversion of CH_4 as a function of porosity.

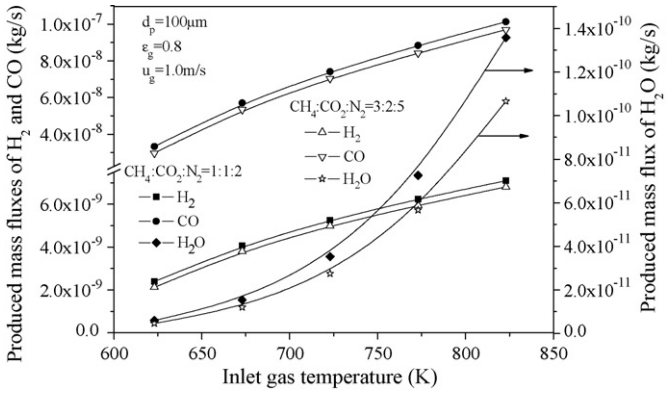

Fig. 10. Profile of produced mass flux of H_2, CO and H_2O as a function of inlet gas temperature.

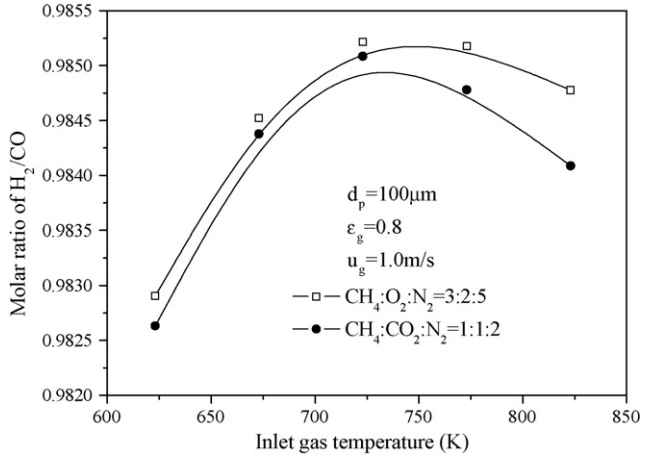

Fig. 11. Profile of ratio of H_2/CO as a function of inlet gas temperature.

3.4. Effect of inlet gas velocity

With the increase of inlet gas velocity, the gas flow passing through the cluster increases. Fig. 12 shows the yields of H_2, CO and H_2O gas species of the cluster as a function of inlet gas velocities. The high inlet gas velocity results in a higher concentration of CH_4 species in the cluster since the gas flux passing through the cluster is increased. The reaction constant

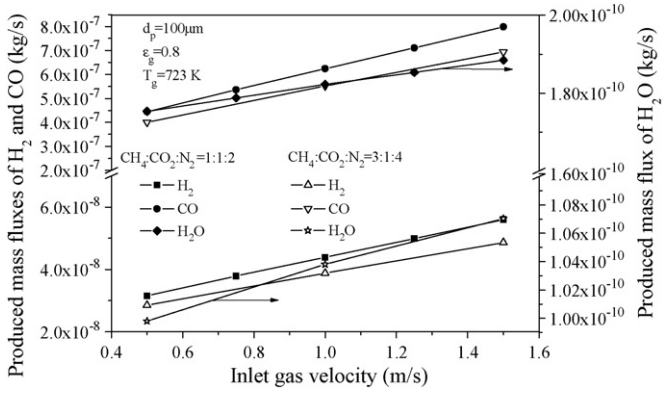

Fig. 12. Profile of produced mass flux of H_2, CO and H_2O as a function of inlet gas velocity.

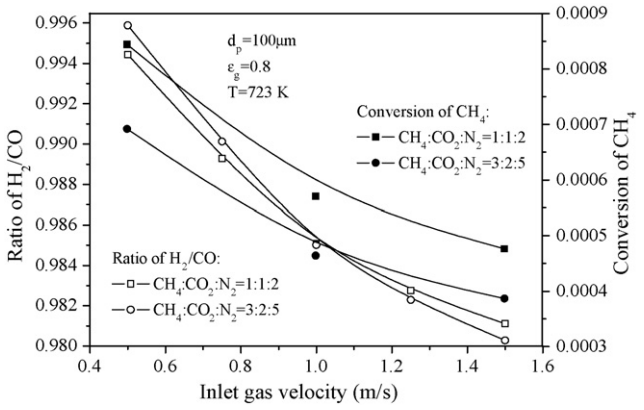

Fig. 13. Distributions of H_2/CO and conversion of CH_4 as a function of inlet gas velocity.

of methane is increased, and the carbon dioxide reforming with methane is promoted. This indicates that the yields of H_2, CO and H_2O alter with the relative velocity between gas and catalyst particle cluster. Note that the velocity passing through the cluster increases with the increase of inlet gas velocity. Perhaps after a certain critical relative velocity is reached, the breakup of the cluster will be taken place. However, this important effect is not possible to investigate using the present model.

Fig. 13 shows the molar ratio of H_2/CO as a function of inlet gas velocity. The conversion of methane was also given in this figure. The low conversion of methane can be attributed to low number of particles in the cluster. As the inlet gas velocity increases, the ratio of H_2/CO monotonously decreases. This is because the dry reforming reaction of methane with carbon dioxide can proceed quickly, but methane reforming with CO_2 cannot reach completion, and the reverse water–gas shift reaction is faster under this reaction condition. In conclusion, the reaction had to be operated at a low velocity to reach high H_2 yield for the endothermic CO_2 reforming of methane.

3.5. Effect of gas pressure

The effect of reactor pressure on concentration distribution of H_2, CO and H_2O is plotted in Fig. 14 by using the kinetic

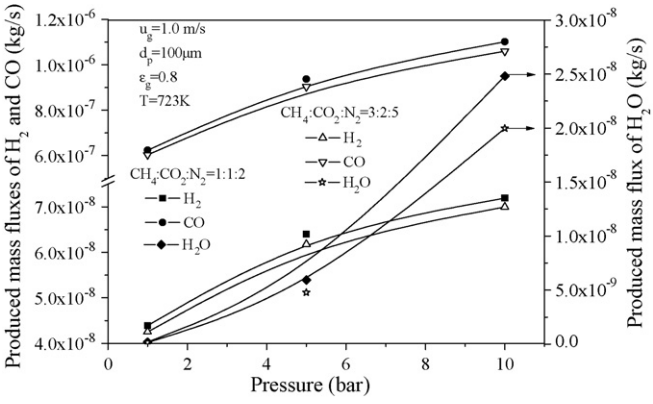

Fig. 14. Profile of produced mass flux of H_2, CO and H_2O as a function of reactor pressure.

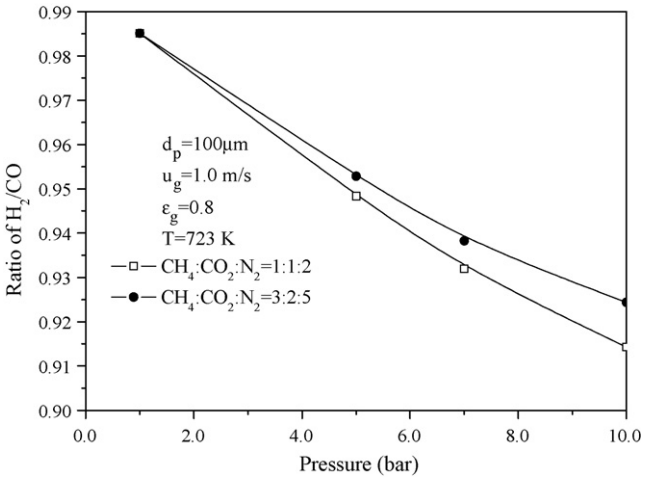

Fig. 15. Ratio of H_2/CO as a function of gas pressure.

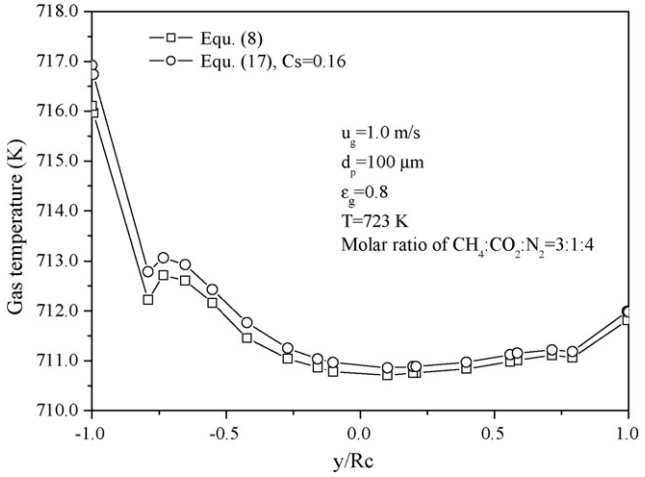

Fig. 16. Distribution of gas temperature along axial direction.

expressions reported in Section 2. The mass fluxes of H_2, CO and H_2O increased with increasing reactor pressure. Increasing the reactor pressure produces an increase in the carbon dioxide reforming with methane and reverse water–gas shift reaction. On the other hand, the gas flux passing through the catalyst particle cluster will be reduced due to high flow resistance caused by gas viscosity and density at high pressure. Hence, the yields of H_2, CO and H_2O species are increased with the increase of reactor pressure.

The effect of the variation of the reactor pressure on the molar ratio of H_2/CO is presented in Fig. 15. It is shown that the reaction rates are strongly affected by the reactor pressure. The ratio of H_2/CO decreased with increasing reactor pressure. These results were expected, as increasing pressure is thermodynamically unfavorable for this reaction system. This result indicates that the carbon dioxide reforming with methane is slower than that the reverse water–gas shift reaction at the high reactor pressure.

3.6. Effect of carbon deposition

Coke may form on the catalyst surface and leads to deactivation of the catalyst via pore blockage. Hence, coke formation is one of the major problems associated with dry reforming [44,45]. The deposition of carbon is mainly due to methane decomposition or CO disproportionation [46–48]. Methane decomposition is an endothermic reaction while carbon monoxide disproportionation is exothermic. As a result of these reactions, the amount of coke formed, depends on the CH_4/CO_2 feed ratio and the operating temperature and pressure. Although the types of coke that occur during reforming are thoroughly reviewed, little is known about the modeling of the carbon formation phenomenon, either from a thermodynamic or kinetic standpoint [49,50]. Ginsburg et al. [50] proposed a kinetic model to predict the rate of coke formation. This type of kinetics strongly suggests the requirement of three adjacent free catalyst sites for the coking reaction to proceed under allowable thermodynamic conditions. By introducing a factor that is the ratio between the experimental reaction constant and the thermodynamic equilibrium constant, the carbon deposition effect was accounted in the reaction model to identify the actual reaction order [51]. The fraction of the active sites covered by methane and carbon were incorporated into the rate of reforming reaction considering four reactions: methane reforming, reverse water–gas shift, carbon deposition, and carbon removal by a reverse Boudouard reaction [52]. Considering the effect of carbon deposition, the reaction rate of methane with carbon dioxide is calculated by introducing a correction coefficient of coke selectivity C_s, where C_s is the moles of coke formed/moles of methane converted:

$$R_A = (1 - C_s)k_A \left[\frac{K_{CO_2} K_{CH_4} P_{CO_2} P_{CH_4}}{(1 + K_{CO_2} P_{CO_2} + K_{CH_4} P_{CH_4})^2}\right] \times \left[1 - \frac{(P_{CO} P_{H_2})^2}{k_A P_{CH_4} P_{CO_2}}\right] \quad (17)$$

Experimental results show that the coke selectivity increases with the increase of flux of methane [50]. Fig. 16 shows the computed distribution of gas temperature along axial direction using Eqs. (8) and (17), respectively. The predicted gas temper-

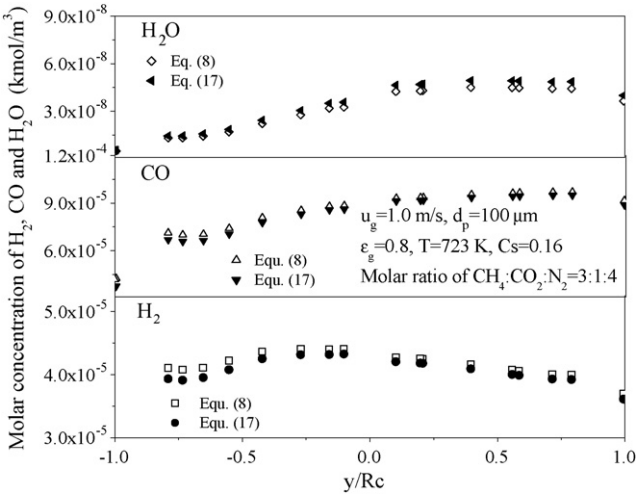

Fig. 17. Distribution of concentration of gas species along axial direction.

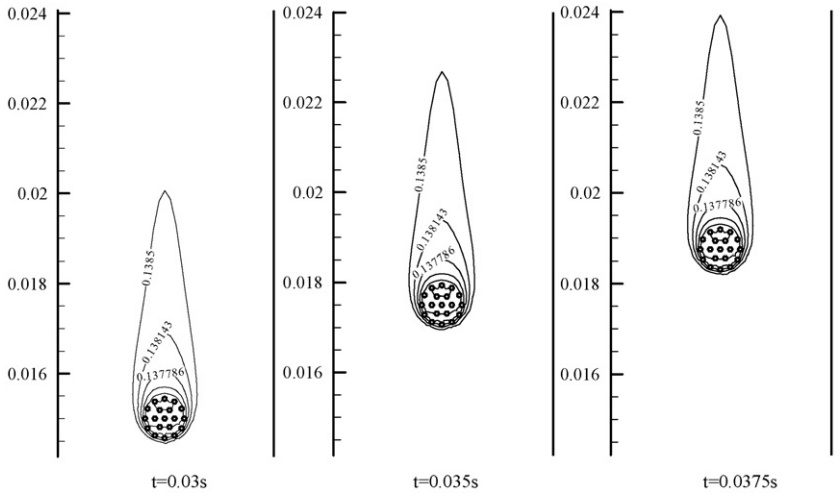

Fig. 18. Contour of molar fraction of CH_4 species at the inlet gas velocity and cluster velocity of 1.5 and 0.5 m/s, and inlet gas temperature of 723 K.

ature is higher if Eq. (17) is used instead of Eq. (8). This means that the carbon deposition will reduce reaction rate of methane with carbon dioxide and as a result the gas temperature is not dropped as much. Fig. 17 shows the distributions of gas species along axial direction. The concentrations of H_2 and CO were reduced, while the concentration of H_2O was increased with the consideration of the effect of carbon depositions. Hence, the coke formation will reduce the conversion of methane.

3.7. Effect of relative motion of cluster

Clusters have been experimentally observed in both the core and annulus regions of vertical risers. Size, shape, velocity, cluster lifetime, frequency of occurrence and wall contact times have been measured or inferred from measurements [21–26]. It is found that cluster travels downward in the annulus whilst it usually moves upward in the core [53]. Subbarao [54] developed a model of mean cluster diameter to predict heat transfer in circulating fluidized beds. The cluster size was a function of bubble size, superficial gas velocity and solids flux. Xu and Li [55] presents an expression for predicting cluster diameter as a function of the suspension density, particle density and particle size. The motion of cluster is stochastic, and the cluster shape is highly variable. For simplicity, we assumed that all particles in the cluster move with the same velocity. Hence, the diameter of cluster during its motion is kept at its original size. Fig. 18 shows the contours of molar concentration of CH_4 species at three instances using the dynamic mesh model via adaptively sampled distance fields [56]. In such computing condition, the inlet gas velocity and cluster velocity are 1.5 and 0.5 m/s, respectively. All particles in the cluster are moving at the constant velocity of 0.5 m/s along axial direction. Hence, the porosity of cluster is constant at 0.8. The relative velocity between gas phase and particles, $(u_g - u_s)$, is 1.0 m/s. The molar fraction of CH_4 is higher in the front compared to the back of the cluster. We found that the distributions of molar fraction of CH_4 are the same at three different times. Fig. 19 shows the distributions of H_2/CO as a function of relative velocity, where gas velocity is 1.5 m/s. As

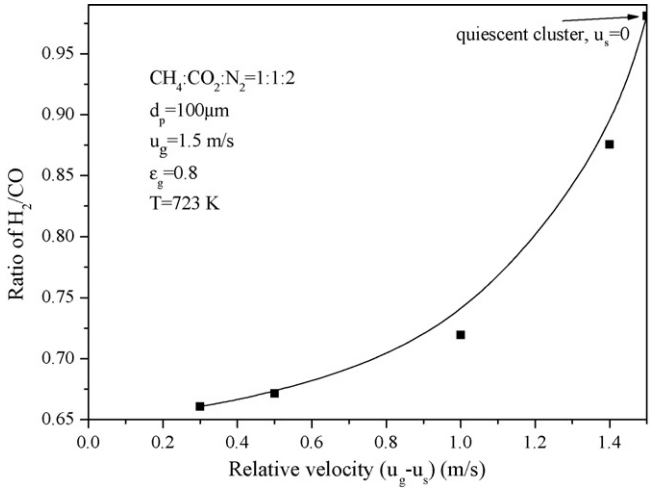

Fig. 19. Ratio of H_2/CO as a function of relative velocity.

the relative velocity increases, the ratio of H_2/CO increases since the gas flux passing through the cluster was increased. Hence, the high conversion of methane is contributed to the high relative velocity between gas and cluster in the circulating fluidized bed reformers.

4. Conclusions

A mathematical model for predicting dry methane reforming has been proposed by coupling hydrodynamics with Rh/Al_2O_3 catalyst particle chemical reactions. Flow behavior of gas passing through the catalyst particle cluster was obtained. Gas flows through the cluster is negligible throughout if porosity is less than 0.9. The force acting on each catalyst particle at various locations in the cluster is significantly different, and is much lower than the case for the isolated catalyst particle.

The H_2 and CO yields increase with the increase of inlet gas velocity and displayed a convex like behavior with increasing of inlet gas temperature. Furthermore, it is found that the carbon dioxide reforming with methane is promoted with the increase

of reactor pressure and the reforming reaction rate is increased also. An increase in the reactor pressure always causes a decrease in molar ratio of H_2/CO.

There are some limitations associated with the present model. First of all, the simulations are all two-dimensional which leads to a vortex structure around the catalyst particle cluster and a decrease in the velocity. Present model also takes a porous medium as the equivalent of a catalyst particle cluster. The porous medium maintains its mechanical structure through the simulations and so the cluster breakup is not simulated. Presently there is not a commercially available software package that can simulate this breakup/shedding phenomena. There is also the assumption that the cluster is shaped as a circular object. This is a good basis for the start of the simulations but it certainly is an approximation. Hence, this model needs to be further refined with more accurate and experimentally verified formulations for modeling dry methane reforming processes in circulating fluidized bed reformers.

Acknowledgements

This work was supported by Natural Science Foundation of China through Grant No. 20606006 and NSFC-Petro China Company Limited under the cooperative Project No. 20490200, and Project (HIT2003.34) supported by the Scientific Research Foundation of Harbin Institute of Technology.

References

[1] E. Ruckenstein, Y. Hu, Combination of CO_2 reforming and partial oxidation of methane over NiO/MgO solid solution catalysts, Ind. Eng. Chem. Res. 37 (1998) 1744–1747.
[2] X.E. Verykios, Catalytic dry reforming of natural gas for the production of chemicals and hydrogen, Int. J. Hydrogen Eng. 28 (2003) 1045–1063.
[3] T. Wurzel, S. Malcus, L. Mleczko, Reaction engineering investigations of CO_2 reforming in a fluidized-bed reactor, Chem. Eng. Sci. 55 (2000) 3955–3966.
[4] E. Ruckenstein, H.Y. Wang, Combined catalytic partial oxidation and CO_2 reforming of methane over supported cobalt catalysts, Catal. Lett. 73 (2001) 99–105.
[5] J. Yaying, W. Li, H. Xu, Catalytic partial oxidation of methane to synthesis gas over Ni/γ-Al_2O_3 catalyst in a fluidized-bed, Appl. Catal. A: Gen. 213 (2001) 25–31.
[6] H.Y. Wang, E. Ruckenstein, CO_2 reforming of CH_4 over Co/MgO solid solution catalysts-effect of calcinations temperature and Co loading, Appl. Catal. A: Gen. 209 (2001) 207–215.
[7] K. Tomishige, Y. Matsuo, Y. Sekine, K. Fujimoto, Effective methane reforming with CO_2 and O_2 under pressurized condition using NiO-MgO and fluidized bed reactor, Catal. Commun. 2 (2001) 11–15.
[8] E. Ruckenstein, Y.H. Hu, Combination of CO_2 reforming and partial oxidation of methane over NiO/MgO solid solution catalysts, Ind. Eng. Chem. Res. 37 (1998) 1744–1747.
[9] C. Zhongxiang, P. Pradeep, Y. Yibin, S. Elnashaie, Simulation for steam reforming of natural gas with oxygen input in a novel membrane reformer, Fuel Process. Technol. 83 (2003) 235–252.
[10] L. Paturzo, F. Gallucci, A. Basile, G. Vitulli, P. Pertici, An Ru-based catalytic membrane reactor for dry reforming of methane-Its catalytic performance compared with tubular packed bed reactors, Catal. Today 82 (2003) 57–65.
[11] A.F. Sammells, M. Schwartz, R.A. Mackay, T.F. Barton, D.R. Peterson, Catalytic membrane reactors for spontaneous synthesis gas production, Catal. Today 56 (2000) 325–328.
[12] T. Hayakawa, A.G. Andersen, M. Shimizu, K. Suzuki, K. Takehira, Partial oxidation of methane to synthesis gas, Catal. Lett. 22 (1993) 307–317.
[13] A.M. Adris, C.J. Lim, J.R. Grace, The fluidized-bed membrane reactor for steam methane reforming: model verification and parametric study, Chem. Eng. Sci. 52 (1997) 1609–1622.
[14] S. Roy, B.B. Pruden, A.M. Adris, C.J. Lim, J.R. Grace, Fluidized-bed steam methane reforming with oxygen input, Chem. Eng. Sci. 54 (1999) 2095–2102.
[15] K. Tomishige, Syngas production from methane reforming with CO_2/H_2O and O_2 over NiO-MgO solid solution catalyst in fluidized bed reactors, Catal. Today 89 (2004) 405–418.
[16] A.K. Prabhu, A. Liu, L.G. Lovell, S.T. Oyama, Modeling of the methane reforming reaction in hydrogen selective membrane reactors, J. Membr. Sci. 177 (2000) 83–95.
[17] P. Pradeep, S.S.E.H. Elnashaie, Coupled steam and oxidative reforming for hydrogen production in a novel membrane circulating fluidized-bed reformer, Ind. Eng. Chem. Res. 42 (2003) 4715–4722.
[18] J. Grace, A.E.M. Adris, T. Boyd, C.J. Lim, Hydrogen from an internally circulating fluidized bed membrane reactor, Int. J. Chem. Reactor Eng. 3 (2005) 1–12.
[19] C. Zhongxiang, S.S.E.H. Elnashaie, Bifurcation and its implications for a novel autothermal circulating fluidized bed membrane reformer for the efficient pure hydrogen production, Chem. Eng. Sci. 60 (2005) 4287–4309.
[20] J. Yerushalmi, N.T. Cankurt, D. Geldart, B. Liss, Flow regimes in vertical gas–solid contact systems, AIChE Symp. Ser. 74 (1978) 1–13.
[21] C.J. Chen, Experiments that address phenomenological issues in fast fluidization, Chem. Eng. Sci. 54 (1999) 5529–5539.
[22] M. Horio, H. Kuroki, Three-dimensional flow visualization of dilutely dispersed solids in bubbling and circulating fluidized beds, Chem. Eng. Sci. 49 (1994) 2413–2421.
[23] V.D. Moortel, E. Azario, R. Santini, L. Tadrist, Experimental analysis of the gas-particle flow in a circulating fluidized bed using a phase Doppler particle analyzer, Chem. Eng. Sci. 53 (1998) 1883–1899.
[24] P.D. Noymer, L.R. Glicksman, Cluster motion and particle-convective heat transfer at the wall of a circulating fluidized bed, Int. J. Heat Mass Transfer 41 (1998) 147–158.
[25] A.K. Sharma, K. Tuzla, J. Matsen, J.C. Chen, Parametric effects of particle size and gas velocity on cluster characteristics in fast fluidized beds, Powder Technol. 111 (2000) 114–122.
[26] S.V. Manyele, J.H. Parssinen, J.X. Zhu, Characterizing particle aggregates in a high-density and high-flux CFB riser, Chem. Eng. J. 88 (2002) 151–161.
[27] V.V. Ranade, Computational Flow Modeling for Chemical Reactor Engineering, Plenum Press, New York, 2001.
[28] G.F. Froment, K.B. Bischoff, Chemical Reactor Analysis and Design, second ed., Wiley, New York, 1990.
[29] K. Kunii, O. Levenspiel, Fluidization Engineering, second ed., Butterworth Heinemann, MA, USA, 1991.
[30] Z. Yunhau, L. Huilin, H. Yurong, J. Ding, Y. Lijie, Numerical prediction of combustion of carbon particle clusters in a circulating fluidized bed riser, Chem. Eng. J. 118 (2006) 1–10.
[31] D.C. Wilcox, Turbulence Modeling for CFD, DEC Ind., La Canada, CA, 1993.
[32] B.E. Launder, D.B. Spalding, Mathematical Models of Turbulence, Academic Press, London, 1972.
[33] J.T. Richardson, S.A. Paripatyadar, Carbon dioxide reforming of methane with supported rhodium, Appl. Catal. 61 (1990) 293–309.
[34] X.E. Verykios, Catalytic dry reforming of natural gas for the production of chemicals and hydrogen, Int. J. Hydrogen Energy 28 (2003) 1045–1063.
[35] X. Jianquo, G.F. Froment, Methane steam reforming, methanation and water–gas shift. I. Intrinsic kinetics, AIChE J. 35 (1989) 88–96.
[36] K. Jarosch, T. El Solh, H.I. de Lasa, Modelling the catalytic steam reforming of methane: discrimination between kinetic expressions using sequentially designed experiments, Chem. Eng. Sci. 57 (2002) 3439–3451.
[37] M.A. Soliman, S.S.E.H. Elnashaie, A.S. Al-Ubaid, A.M. Adris, Simulation of steam reformers for methane, Chem. Eng. Sci. 43 (1988) 1801–1806.
[38] D. Dissanayake, M.P. Rajput, B. Prabhakar, Low temperature oxidative conversion of methane to syngas over NiO-CaO catalyst, Catal. Lett. 15 (1991) 363–370.

[39] W. Jin, X. Gu, S. Li, P. Huang, N. Xu, J. Shi, Experimental and simulation study on a catalyst packed tubular dense membrane reactor for partial oxidation of methane to syngas, Chem. Eng. Sci. 55 (2000) 2617–2625.
[40] H. Yurong, L. Huilin, S. Qiaoqun, Y. Lidan, Z. Yunhua, D. Gidaspow, J. Bouillard, Hydrodynamics of gas–solid flow around immersed tubes in bubbling fluidized beds, Powder Technol. 145 (2004) 88–105.
[41] J.C. Moran, L.R. Glicksman, Experimental and numerical studies on the gas flow surrounding a single cluster applied to a circulating fluidized bed, Chem. Eng. Sci. 58 (2003) 1879–1886.
[42] A. Gadalla, M. Sommer, Carbon dioxide reforming of methane on nickel catalysts, Chem. Eng. Sci. 44 (1989) 2825–2829.
[43] V.A. Tsipouriari, X.E. Verykios, Kinetic study of the catalytic reforming of methane with carbon dioxide to synthesis gas over Ni/La_2O_3 catalyst, Catal. Today 64 (2001) 83–90.
[44] T.E. Solh, K. Jarosch, H. de Lasa, Catalytic dry reforming of methane in a CREC riser simulator kinetic modeling and model discrimination, Ind. Eng. Chem. Res. 42 (2003) 2507–2515.
[45] K. Tomishige, Y. Himeno, Y. Matsuo, Y. Yoshinaga, K. Fujimoto, Catalytic performance and carbon deposition behavior of a NiO-MgO solid solution in methane reforming with carbon dioxide under pressurized conditions, Ind. Eng. Chem. Res. 39 (2000) 1891–1897.
[46] H.M. Swaan, V.C.H. Kroll, G.A. Martin, C. Mirodatos, Deactivation of supported nickel catalysts during the reforming of methane by carbon dioxide, Catal. Today 21 (1994) 571–578.
[47] Z.L. Zhang, X.E. Verykios, Carbon dioxide reforming of methane to synthesis gas over Ni/La_2O_3 catalysts, Appl. Catal. A: Gen. 138 (1996) 109–133.
[48] K. Tomishige, Y.G. Chen, K. Fujimoto, Studies on carbon deposition in CO_2 reforming of CH_4 over nickel-magnesia solid solution catalysts, J. Catal. 181 (1999) 91–103.
[49] J.R. Rostrup-Nielsen, Industrial relevance of coking, Catal. Today 37 (1997) 225–232.
[50] J.M. Ginsburg, J.L. Pin, T.E. Solh, H.I. de Lasa, Coke formation over a nickel catalyst under methane dry reforming conditions: thermodynamic and kinetic models, Ind. Eng. Chem. Res. 44 (2005) 4846–4854.
[51] I. Tavazzi, A. Beretta, G. Groppi, P. Forzatti, Development of a molecular kinetic scheme for methane partial oxidation over a $Rh/\alpha\text{-}Al_2O_3$ catalyst, J. Catal. 241 (2006) 1–13.
[52] V.I. Mahesh, P.N. Lawrence, L.K. Edwin, B.D. Dady, Kinetic modeling for methane reforming with carbon dioxide over a mixed-metal carbide catalyst, Ind. Eng. Chem. Res. 42 (2003) 2712–2721.
[53] W. Shuyan, L. Huanpeng, L. Huilin, L. Wentie, J. Ding, L. Wei, Flow behavior of clusters in a riser simulated by direct simulation Monte Carlo method, Chem. Eng. J. 106 (2005) 197–211.
[54] D. Subbarao, Cluster and lean phase behavior, Powder Technol. 46 (1986) 101–107.
[55] G. Xu, J. Li, Analytical solution of the energy minimization multiscale model for gas–solid two-phase flow, Chem. Eng. Sci. 53 (1998) 1349–1366.
[56] P.L. George, H. Borouchaki, P. Laug, An efficient algorithm for 3D adaptive meshing, Adv. Eng. Software 33 (2002) 377–387.